Journal of Mathematics in Industry (2011) 1:1
DOI 10.1186/2190-5983-1-1

Journal of Mathematics in Industry
a SpringerOpen Journal

RESEARCH Open Access

Acid polishing of lead glass

Jonathan A Ward · Andrew C Fowler · Stephen BG O'Brien

Received: 11 November 2010 / Accepted: 3 June 2011 / Published online: 3 June 2011

Abstract *Purpose:* The polishing of cut lead glass crystal is effected through the dowsing of the glass in a mixture of two separate acids, which between them etch the surface and as a result cause it to be become smooth. In order to characterise the resultant polishing the rate of surface etching must be known, but when this involves multicomponent surface reactions it becomes unclear what this rate actually is.
Methods: We develop a differential equation based discrete model to determine the effective etching rate by means of an atomic scale model of the etching process.
Results: We calculate the etching rate numerically and provide an approximate asymptotic estimate.
Conclusions: The natural extension of this work would be to develop a continuum advection-diffusion model.

Keywords Etching rate multi-component · crystal glass · mathematical model · ordinary differential equation · asymptotics · numerics · Laplace transform

1 Introduction

Wet chemical etching, or chemical milling, is a technique which allows the removal of material from a substrate via chemical reaction. In many applications selective attack by the chemical etchant on different areas of the substrate is controlled by removable layers of masking material or by partial immersion in the etchant. Etching is used in

JA Ward · AC Fowler · SBG O'Brien (✉)
MACSI, Department of Mathematics and Statistics, University of Limerick, Limerick, Ireland
e-mail: stephen.obrien@ul.ie

JA Ward
e-mail: jonathan.ward@ul.ie

AC Fowler
e-mail: andrew.fowler@ul.ie

a wide variety of industrial applications, from the manufacture of integrated circuits to the fabrication of glass microfluidic devices [1–4]. Stevens [5] gives a qualitative description of etching in the context of tool design, masks for television tubes and fine structures in microelectronics. More recent accounts are to be found in [6, 7], who also include a detailed examination of the chemistry of these processes. In this paper we wish to examine the etching of rough lead crystal glass fully immersed in a bath of acid etchant. The evolution of the surface is determined by the rate of the surface reaction which dissolves the solid surface. For a simple reaction involving a single solvent and a monominerallic surface, this rate is simply characterised by the reaction rate kinetics. However, if more than one solvent is necessary to dissolve a surface with several different components, it is not clear what the effective surface dissolution rate should be.

This paper is concerned with this latter situation, and is motivated by *multicomponent* etching used in the production of lead crystal glassware. This problem was introduced at a European study group for industry at the university of Limerick in 2008 (ESGI 62). In this case, decorative features cut into the glass leave it optically opaque and polishing is subsequently required to restore its transparency [1]. The process consists of sequential immersion of the glass in a mixture of hydrofluoric (HF) and sulphuric (H_2SO_4) acid, followed by rinsing to remove insoluble lead sulphate particles from the interface. The etching and rinsing steps are repeated a number of times. In particular, we focus on the wet chemical etching step, where it is necessary to use both hydrofluoric and sulphuric acid in order to dissolve all of the components of the glass, namely SiO_2, PbO and K_2O. The potassium salts and silicon tetrafluoride are soluble whereas the lead sulphate is not, hence the required rinsing. Such multicomponent systems pose a non-trivial problem in determining the consequent etching rate [8].

There is a large literature concerning experimental studies of wet chemical etching of glass; see [1], for a review. These studies are primarily concerned with the measurement of etching rates [2] and how these are related to different etchant and glass compositions [3, 9, 10]. It has been shown that etching rates of multicomponent glasses, where all the components dissolve in HF, have a non-trivial dependence on both the 'bonding connectivity' of the glass and the presence of reaction by-products on its surface [10]. To our knowledge, there has not been an experimental study of multicomponent glasses where different types of etchant are required. An observation related to the work in this paper is that etching of a smooth surface (for example, one which has been mechanically polished) causes it to develop cusp like features [1, 3], thus roughening it slightly. The height of such features is found to be normally distributed [11].

In the mathematics literature, the simplest models of macroscopic surface evolution have been well studied [12]. A closely related process involves erosion via powder blasting [13]. In general, if a surface is given by $F(\mathbf{x}, t) = 0$, then its velocity $\mathbf{v}$ satisfies $F_t + \mathbf{v}.\nabla F = 0$, whence also $F_t + v_p|\nabla F| = 0$, where $v_p = \mathbf{v}.\mathbf{n}$ denotes the normal velocity of the surface, and $\mathbf{n} = \frac{\nabla F}{|\nabla F|}$ is the unit normal. For example, if the surface is denoted by $z = s(x, y, t)$, then (taking $F = s - z$)

$$s_t = -\left[1 + |\nabla s|^2\right]^{1/2} v_p, \tag{1.1}$$

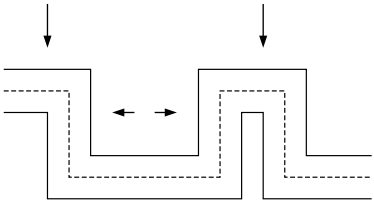

Fig. 1 Cartoon of etching if the rate of erosion is constant and normal to the surface. The surface is represented at three different times. Peaks are sharpened (before disappearing), troughs are broadened.

where v_p is the removal rate of the surface normal to itself. If v_p were approximately constant, qualitatively we would then expect the process to proceed as in Figure 1 where part of a surface feature is sketched at three times. Peaks would be sharpened and troughs broadened; the sharpened peaks will disappear rapidly because of their larger surface/volume ratio; the average etching depth required to achieve a smooth surface will be of the order of the initial peak-to-trough amplitude of the roughness.

We might also postulate that the normal velocity v_p will depend on elastic strain energy and curvature; such effects have been considered in stressed media [14–16]. We would then expect the reaction rate to increase with the curvature of the surface (and acid concentration). Specifically, the mean curvature of the surface κ is defined by

$$2\kappa = \nabla.\mathbf{n} = -\nabla.\left[\frac{\nabla s}{(1+|\nabla s|^2)^{1/2}}\right], \tag{1.2}$$

and thus

$$s_t = -\left[1+|\nabla s|^2\right]^{1/2} v_p(\kappa), \tag{1.3}$$

where v_p is an increasing function of the curvature κ: a first approximation might take the form $v_p(\kappa) = v_{p0}(1+\alpha\kappa)$. Hence (1.3) is a non-linear diffusion equation for s. As such, the surface will smooth as it is etched, and this would explain simply enough why polishing works. From an experimental point of view, halting the etching processes at various times and examining the surface microscopically is an obvious way of testing the validity of the above mechanisms. The latter mechanism will generally give surfaces which are progressively smoother while the former (constant v_p) could lead to the development of intermediate cusps prior to the ultimate removal of asperities.

For a single component system, Kuiken [17] considered the problem of selective removal by etching of material from a substrate partially covered with a mask (cf. engraving). He developed a two dimensional model on an infinite domain (half mask, half substrate) for the diffusion limited case near a resistant edge (that is, when the transport of the active species occurs primarily by diffusion), and obtained approximate solutions using a matched asymptotic expansions approach. The (etching) velocity was taken to be proportional to the concentration gradient (but independent of the surface curvature), that is,

$$\mathbf{v} = -\sigma_e \nabla c, \tag{1.4}$$

where $\mathbf{v}$ is the etching rate, σ_e is a constant and c is the etchant concentration. He then refined this model to deal with the case of a mask with a finite hole [18]. Later, this

approach was further developed and successfully compared with experiment [19]. While this might suggest, at least in the system they considered, that the dependence of etching rate on surface energy is weak, it should also be noted that the substrate to be etched was initially smooth. The etching of lead glass is different in that the initial substrate has a rough surface of high curvature.

The glass polishing process involves the dissolution of cut glass surfaces in a reservoir of hydrofluoric acid (HF) and sulphuric acid (H_2SO_4). Lead crystal consists largely of lead oxide PbO, potassium oxide K_2O, and silica SiO_2, and these react with the acids according to the reactions

$$\begin{aligned} \mathrm{PbO} + \mathrm{H_2SO_4} &\xrightarrow{r_1} \mathrm{PbSO_4} + \mathrm{H_2O}, \\ \mathrm{SiO_2} + 4\mathrm{HF} &\xrightarrow{r_2} \mathrm{SiF_4} + 2\mathrm{H_2O}, \\ \mathrm{K_2O} + \mathrm{H_2SO_4} &\xrightarrow{r_3} \mathrm{K_2SO_4} + \mathrm{H_2O}, \\ \mathrm{K_2O} + 2\mathrm{HF} &\xrightarrow{r_4} 2\mathrm{KF} + \mathrm{H_2O}. \end{aligned} \tag{1.5}$$

The surface where the reaction occurs is a source for the substances on the right hand side and a sink for those on the left hand side. The potassium salts are soluble, as is the silicon hexafluoride, but the lead sulphate is insoluble and precipitates on the cut surface, from which it is washed away in the rinsing bath. In fact this rinsing action must be chemical, with the water acting to dissolve the bonds which tie the sulphate crystals to the surface.

Spierings [1] points out that the mechanism of the etching reaction is not well understood at molecular level: our aim in this paper is to elaborate upon previous work [8] where we proposed a *microscopic* model to capture the salient features of multicomponent etching, with the aim of determining the effective etching rate.

The outline of the paper is as follows. In the section 'Modelling multicomponent etching' we discuss the mechanical process of etching, in particular where more than one solvent is necessary, and we indicate a conundrum which arises in this case. We then build a model which describes the evolution of the surface at an atomic scale, describing in particular the evolution of atomic scale surface roughness. This model is solved in the section 'Solution of the discrete model', and the resulting effective etching rate is determined. A feature of the solution is that, although the model describes the evolution of a site occupation density on a discrete lattice, the numerical solutions strongly suggest that a continuum approximation should be appropriate. In the section 'A continuum model', we derive such a model and study its solutions. Surprisingly, we find that the consequent etching rate differs from that computed from the discrete model, and we offer an explanation for why this should be so. The conclusions follow in the last section.

2 Modelling multicomponent etching

2.1 Etching rate

We first need to relate the etching rate v_p to the reaction rates of (1.5) neglecting curvature effects. We will assume that the chemical reactions at the surface form

the rate-determining step in the process and the reaction products are also quickly removed from the surface. We denote the reaction rates of the four reactions in (1.5) as r_1, r_2, r_3 and r_4, respectively, with units of moles per unit area per unit time. Denote further the densities of lead oxide, silica and potassium oxide by ρ_P, ρ_S and ρ_K, respectively, their volume fractions within the glass by ϕ_P, ϕ_S and ϕ_K, and their molecular weights by M_P, M_S and M_K. Then the density of species j in the glass is $\phi_j \rho_j$, and its molar density (moles per unit volume) is

$$m_j = \frac{\phi_j \rho_j}{M_j}. \tag{2.1}$$

Therefore if v_p is the rate of erosion of the surface, the rate at which species j disappears from the surface is $\frac{\phi_j \rho_j v_p}{M_j}$, and this must be equal to the rate of disappearance R_j for each species in the glass, measured in moles per unit area of surface per unit time. (Thus R_j has the units of a molar flux.) Hence

$$\frac{\phi_i \rho_i v_p}{M_j} = R_j. \tag{2.2}$$

In terms of the reaction rates r_j of (1.5), we would have

$$R_P = r_1, \quad R_S = r_2, \quad R_K = r_3 + r_4. \tag{2.3}$$

If we define

$$m = \sum_j m_j \tag{2.4}$$

to be the average molar density of all three species, that is, of the glass, then

$$f_j = \frac{m_j}{m} \tag{2.5}$$

is the fraction of sites in the glass occupied by species j. Assuming that there is always an excess of acid available for reaction with the three species in the glass, it is natural to assume the balance

$$R_j = f_j F_j, \tag{2.6}$$

where F_j is the effective flux of external (acid) reactant to the surface to react with species j, and thus (2.2) and (2.6) imply

$$m v_p = F_j. \tag{2.7}$$

While this is a statement that the flux of acid to the surface exactly balances the 'flux' of surface disappearing via chemical reaction, it leads us to what we will call the Tocher conundrum. (This observation was made by Dave Tocher during ESGI 62 at the University of Limerick.) The mathematical part of this conundrum lies in the general impossibility of satisfying (2.7) for each species, since it would require the specific effective reaction rates F_i to be related to each other, and this is unrealistic.

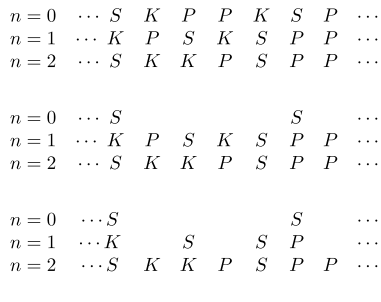

Fig. 2 Cartoon of a portion of a lattice consisting of three types of molecules K, P, S at three different times $t = 0, T, 2T$. In the portion illustrated, $N = 2$, so there are three layers, $n = 0, 1, 2$, and $M = 7$ horizontal sites. For simplicity it is assumed that it takes T seconds to etch a P and K molecule while S is not etched by this acid.

In order to determine what the etching rate v_p is, we thus need to consider in greater detail just what the surface reaction process is.

The Tocher conunudrum follows from the observation that if one of the acids is not present, etching will not occur. For example, one can store sulphuric acid in a glass jar without damage; the hydrofluoric acid is also necessary to cause etching. And yet, the sulphuric acid must attack the lead and potassium oxides. Physically, we can explain the Tocher conundrum in the presence of a single acid, say H_2SO_4, by means of the following conceptual picture. Imagine the glass as a crystal lattice (this is not actually the case, being a glass, but the concept is valid), where lead sulphate, silica and potassium oxide molecules are distributed at random. The sulphuric acid can pick off the lead oxide molecules, and we suppose that it can excavate downwards into the lattice until it encounters a silica molecule. At this point, no further stripping is possible, and reaction at that horizontal location ceases. This stripping will happen at each point of the surface, and, supposing only vertical excavation is possible, eventually a molecularly rough surface will be obtained, in which only silicon molecules are exposed, thus preventing any further reaction. This process is represented qualitatively in Figure 2.

2.2 Microscopic model development

In order to describe the surface reaction, we need to account for the molecularly rough surface, and to do this, we again suppose that the molecules are arranged in a lattice, with the horizontal layers denoted by an index n, with $n = 0$ indicating the initial surface, and n increasing with depth into the lattice. As etching proceeds, the surface will have exposed sites at different levels. We let ψ_n^j denote the fraction of exposed surface at level n of species j.

To clarify this, let us assume there are M sites in the horizontal and $N + 1$ rows in the vertical (see Figure 2) so that $n = 0, \ldots, N$. Then ψ_n^j, at any level or row, n, is the number of exposed sites of type j divided by M.

In addition, the system is evolving in time so $\psi_n^j = \psi_n^j(t)$. As before, the specific effective reaction rate of species j is denoted F_j, and the species is present in a fraction of sites f_j in the crystal (that is, $f_j =$ number of j molecules divided by $M(N + 1)$). Thus

$$\sum_j f_j = 1. \tag{2.8}$$

We define

$$\psi_n = \sum_j \psi_n^j \tag{2.9}$$

to be the fraction of exposed sites at level n (that is, the number of exposed sites at level n divided by the total number of sites N in any row). For example, we illustrate a three species case in Figure 2. At $t = T$, that is, in the middle section of Figure 2, we see that

$$\psi_0^K = \psi_0^P = 0, \quad \psi_0^S = 2/7, \quad \psi_1^K = 1/7, \quad \psi_1^P = 2/7, \quad \psi_1^S = 2/7 \tag{2.10}$$

with all other ψ_n^j being zero.

While one can conceive of a discrete (in time) model where it takes a finite time to etch away a particular molecule, we will take a simpler approach by developing a continuous in time model where we assume an exponential decay law allowing for the time taken for the acid to migrate to and etch any particular molecule. The reaction equations are then ordinary differential equations, describing the time evolution of exposed sites, and are (summation convention not used):

$$\begin{aligned} \dot{\psi}_n^j &= -A_j \psi_n^j + f_j \sum_k A_k \psi_{n-1}^k, \quad n \geq 1, \\ \dot{\psi}_0^j &= -A_j \psi_0^j. \end{aligned} \tag{2.11}$$

The negative term in (2.11) represents the reactive rate of removal of exposed j sites, while the positive term represents the creation of new exposed sites at level n (a fraction f_j of which are j sites) as sites at level $n-1$ are etched away. The initial conditions are simply:

$$\psi_0^j = f_j; \qquad \psi_n^j = 0, \quad n \geq 1. \tag{2.12}$$

If one considers the glass to have finite depth $n = N$, say, then it is necessary to modify the equation for the evolution of ψ_N^j in (2.11) (by removing the first term on the right hand side which represents removal of exposed j sites) to replicate an impenetrable substrate. Thus for simplicity, and mindful of the fact that each level represents a layer of molecules, we consider the glass to be infinitely deep in effect. Note that (2.11) and (2.12) imply the conservation law:

$$\left(\sum_j \sum_n \dot{\psi}_n^j(t) \right) = 0 \Longrightarrow \sum_j \sum_n \psi_n^j(t) = 1. \tag{2.13}$$

The A_j factors, where $j = P, S, K$ corresponds to lead, silicon or potassium, model the rate at which the acid etchant breaks down the j molecules. Thus, for example, $A_S = 0$ if the acid is H_2SO_4 (which does not break down SiO_2 molecules, see (1.5)). The A_j (units s^{-1}) are given by

$$A_j = N F_j (\Delta x)^2, \tag{2.14}$$

where N is Avogadro's number (6×10^{23} mole^{-1}), and Δx is the lattice spacing (m). Note that the molar density is

$$m = \frac{1}{N(\Delta x)^3}, \tag{2.15}$$

so that (2.14) is

$$A_j = \frac{F_j}{m\Delta x}. \tag{2.16}$$

Thus (2.7) leads to an apparent conundrum

$$v_p = A_j \Delta x, \tag{2.17}$$

unless the A_j's are equal.

3 Solution of the discrete model

The evolution of the system is thus described by the system:

$$\begin{aligned} \dot{\psi}_0^j &= -A_j \psi_0^j, \\ \dot{\psi}_n^j &= -A_j \psi_n^j + f_j \sum_k A_k \psi_{n-1}^k, \quad n \geq 1, \end{aligned} \tag{3.1}$$

with initial conditions:

$$\psi_0^j(0) = f_j, \qquad \psi_n^j(0) = 0, \quad n \geq 1. \tag{3.2}$$

3.1 Numerical solution

It is straightforward to solve this system of ordinary differential equations numerically. In Figure 3, we show the time evolution curves into the first three layers of the solid for the case where there are two species 1 and 2 being etched by a single acid. Figure 4 shows a typical solution for the fraction of exposed sites as a function of depth into the crystal at large times. We see that the 'interface' (where ψ_n^j, the fraction of exposed sites at depth n into the crystal of type j, is positive) is diffuse (that is, it spreads out as it moves down into the crystal), and propagates downwards at an essentially constant rate. Note also that the discrete solution appears to be well approximated by a continuously varying site occupation density for each species.

3.2 Analysis of the discrete model

To solve the equations (3.1), we define the Laplace transform of ψ_n^j as

$$\Psi_n^j = \int_0^\infty \psi_n^j e^{-\lambda t}\, dt, \tag{3.3}$$

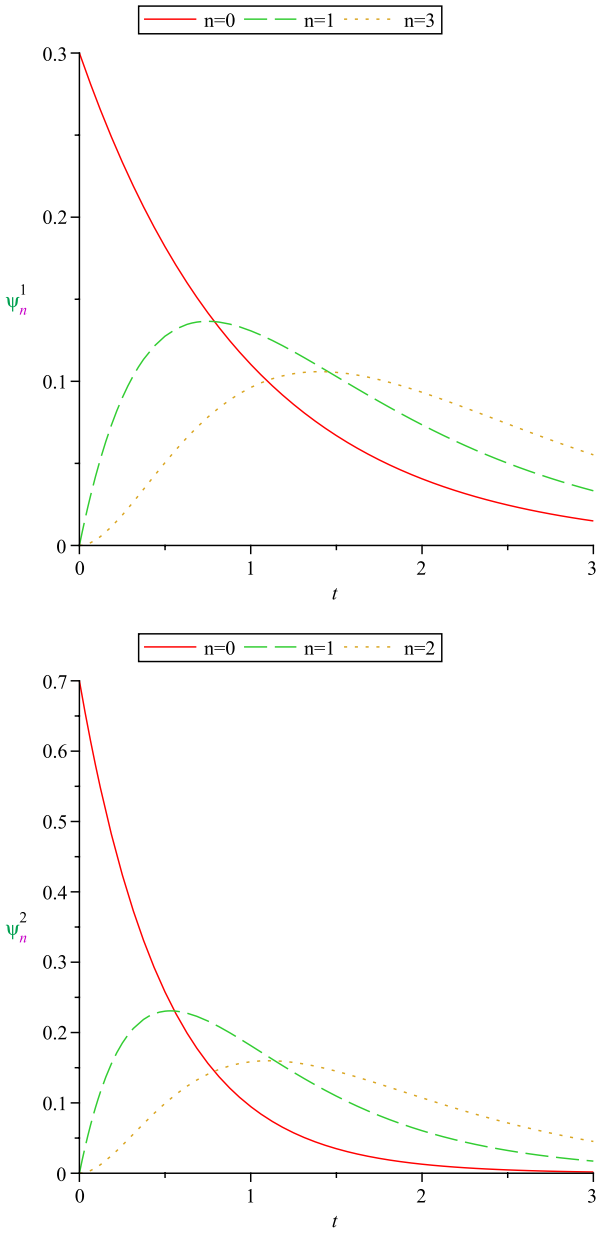

Fig. 3 $\psi_n^1(t)$ and $\psi_n^2(t)$, $n = 0, \ldots, 2$, that is, the time evolution of the fraction of exposed surface of two species 1 and 2 in the first three layers of the crystal ($n = 0, 1, 2$) with initial fractions $f_1 = 0.3$, $f_2 = 0.7$, and respective etching rates $A_1 = 1$, $A_2 = 2$.

so that the equations (3.1) become

$$\begin{aligned} \Psi_0^j &= \frac{f_j}{\lambda + A_j} \quad \text{and} \\ \Psi_n^j &= \frac{f_j}{\lambda + A_j} \sum_k A_k \Psi_{n-1}^k, \quad n \geq 1, \end{aligned} \tag{3.4}$$

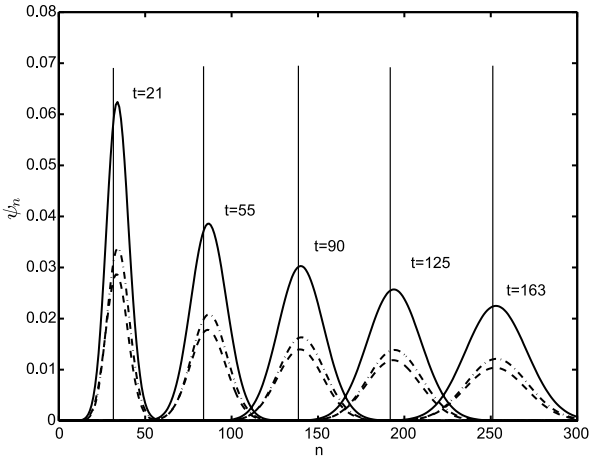

Fig. 4 Simulation results for the solution of (3.1) and (3.2), using two species, with initial fractions $f_1 = 0.3$, $f_2 = 0.7$, and respective etching rates $A_1 = 1$, $A_2 = 2$. The vertical axis represents the fraction of exposed sites at a number of different times; the horizontal axis represents depth into the crystal ($n = 0$ is the top of the crystal). The Gaussian-like curves represent the fraction of vacant sites at level n, that is, ψ_n; dashed curves represent the fraction of vacant sites of species 1 at level n, that is, ψ_n^1; dot-dash curves represent fraction of vacant sites of species 2 at level n, that is, ψ_n^2. The vertical lines represent the asymptotic approximation (3.27) for the position of the wavefront, $n_w \sim 1.54t$, neglecting its diffusion.

respectively. To solve this, define the function

$$g(\lambda) = \sum_k \frac{A_k f_k}{\lambda + A_k}; \tag{3.5}$$

by induction, we then find that

$$\Psi_n^j = \frac{f_j}{\lambda + A_j} g(\lambda)^n. \tag{3.6}$$

Solutions ψ_n^j are found by taking the inverse Laplace transform,

$$\psi_n^j = \frac{1}{2\pi \mathrm{i}} \int_\Gamma \frac{f_j}{\lambda + A_j} g(\lambda)^n e^{\lambda t}\, d\lambda, \tag{3.7}$$

where the contour $\Gamma = [\gamma - i\infty, \gamma + i\infty]$ lies to the right of the poles of the integrand (for example, take $\gamma = 0$). From (3.5) and (3.7), these are

$$\lambda = -A_k. \tag{3.8}$$

The integral (3.7) can be solved explicitly by calculating the residues at the poles $-A_k$. First note that we can write, for any value of s,

$$(\lambda + A_s) g(\lambda) = f_s A_s + (\lambda + A_s) g_s(\lambda), \tag{3.9}$$

where

$$g_s(\lambda) = \sum_{k \neq s} \frac{f_k A_k}{\lambda + A_k}, \tag{3.10}$$

from which it follows that, for any s,

$$g(\lambda)^n = \sum_{r=0}^{n} \frac{{}^nC_r (f_s A_s)^r g_s(\lambda)^{n-r}}{(\lambda + A_s)^r}. \tag{3.11}$$

Since g_s is regular at $-A_s$, we can use (3.11) to determine the coefficients of the Laurent series expansion of (3.7). We can therefore calculate the residues r_{jk} of the integrand of (3.7) at $-A_k$ as

$$\begin{aligned} r_{jj} &= f_j G_j^n e^{-A_j t}, \\ r_{jk} &= \frac{n f_j f_k A_k}{A_j - A_k} G_k^{n-1} e^{-A_k t}, \quad k \neq j, \end{aligned} \tag{3.12}$$

where

$$G_j = g_j(-A_j) = \sum_{l \neq j} \frac{f_l A_l}{A_l - A_j}. \tag{3.13}$$

We then have the explicit formula

$$\psi_n^j = \sum_k r_{jk}. \tag{3.14}$$

Suppose that the species j are ordered in terms of increasing reaction rate so that $A_1 < A_2 < \cdots$; it then follows that at large t,

$$\psi_n^j \sim r_{j1} \sim \begin{cases} f_1 G_1^n e^{-A_1 t}, & j = 1, \\ \dfrac{n f_j f_1 A_1}{A_j - A_1} G_1^{n-1} e^{-A_1 t}, & j > 1, \end{cases} \tag{3.15}$$

for each fixed n. Since (3.13) implies that $G_1 > 0$, it follows that there are two cases to consider. If $G_1 < 1$ then solutions decay in both n and t, but this tells us nothing about the mean etching rate. When $G_1 > 1$, (3.15) indicates that ψ_n^j increases with n; however, this asymptotic result must become inappropriate when $n \sim t$, since conservation of sites implies

$$\sum_j \sum_{n=0}^{\infty} \psi_n^j \equiv 1, \tag{3.16}$$

as in (2.13). Thus ψ_n^j is bounded and in fact decreases towards zero at large n. We wish to focus attention on the penetration depth, or wavefront location, of the etchant so we will denote its location by $n_w(t)$.

3.2.1 *Solutions for large n and t*

To examine the large time behaviour when the penetration depth $n_w \sim t$, we use asymptotic methods to determine the behaviour of ψ_n^j as $t \to \infty$ directly from the integral in (3.7). From Figure 4, we see that the site densities ψ_n^j appear to spread at a constant rate and diffuse as they propagate. This suggests making the ansatz

$$n_w = v_p t + \xi\sqrt{t}, \tag{3.17}$$

where $v_p > 0$, and we will consider the asymptotic form of (3.7) for large t with v_p and ξ fixed. In particular, we will choose v_p to be the speed of the wavefront. We define

$$\rho(\lambda) = \lambda + v_p \ln g(\lambda), \tag{3.18}$$

so that (3.7) takes the form

$$\psi_n^j = \frac{1}{2\pi \mathrm{i}} \int_\Gamma \frac{f_j}{\lambda + A_j} \exp[t\rho + \sqrt{t}\xi \ln g]\, d\lambda. \tag{3.19}$$

Suppose that there are J species. The integrand of (3.19) has poles at $-A_1, -A_2, \ldots, -A_J$, at which g is infinite; between these values, g is monotonically decreasing, and therefore g has $J-1$ real zeroes at $\lambda_1, \ldots, \lambda_{J-1}$, where $-A_j > \lambda_j > -A_{j+1}$. It follows from this that

$$\mathrm{Re}\,\rho = \lambda + v_p \ln|g| \tag{3.20}$$

has $2J-1$ logarithmic branch points at $-A_j$ and λ_k; also since g is convex and decreasing for $\lambda > -A_1$, it follows that ρ is real and convex for $\lambda > -A_1$, with a unique minimum at $\lambda = \lambda^*$, say. The form of $\mathrm{Re}\,\rho$ as a function of λ is shown in Figure 5.

To evaluate the integral (3.19) asymptotically for large t, we aim to deform the contour $\Gamma = [\gamma - i\infty, \gamma + i\infty]$ to one passing through a saddle point of $\rho(\lambda)$, where

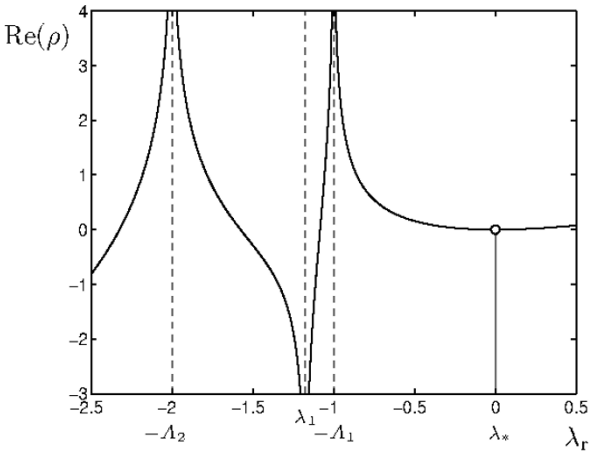

Fig. 5 Example of a plot of $\mathrm{Re}(\rho)$ along the real axis for the two species example illustrated in Figures 3 and 4 ($f_1 = 0.3$, $f_2 = 0.7$, $A_1 = 1$ and $A_2 = 2$) with $v_p = 1.54$. Poles of $\mathrm{Re}(\rho)$ are indicated with dashed grey lines and occur at $-A_1$, $-A_2$ (both poles of g) and λ_1 (zero of g). The minimum at λ_* (solid grey line) is a saddle point in the complex λ plane through which we must deform the integration contour when applying the method of steepest descents (see Figure 6).

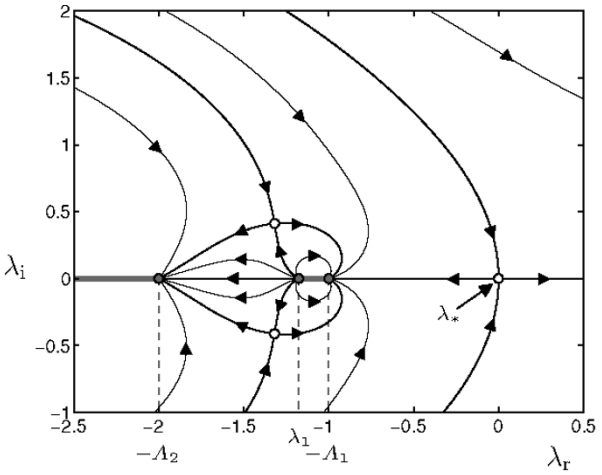

Fig. 6 Contour plot of $\mathrm{Im}(\rho)$ in the complex λ plane for the two species example illustrated in Figures 3, 4 and 5 with $v_p \approx 1.54$. (The appropriate choice of v_p is given by (3.24).) Poles and saddle points are indicated by grey and white markers respectively; branch cuts are labelled with thick grey lines. Arrows indicate the direction of increasing $\mathrm{Re}(\rho)$.

$\rho'(\lambda) = 0$, since the size of the exponent in the integrand is dominated by ρ. We can then use the method of steepest descents. The obvious such saddle point is at λ^*, and this is indeed the correct choice. To understand why, we need to describe the steepest ascent and descent paths in the complex λ plane.

These are given by the curves $\mathrm{Im}\,\rho = \text{constant}$, which trace out trajectories in the complex λ 'phase plane'. (If we think of ρ as a complex velocity potential, then the curves $\mathrm{Im}\,\rho = \text{constant}$ are the streamlines.)

With arrows denoting direction of increasing $\mathrm{Re}\,\rho$ on these curves, the points $-A_j$ are like sinks ($\mathrm{Re}\,\rho \to -\infty$), and the points λ_k are like sources ($\mathrm{Re}\,\rho \to \infty$). On the real axis, the source lines from $(-\infty, \lambda_{J-1}, \ldots, \lambda_1, \lambda^*)$ are directed to the sinks at $-A_j$, as shown in Figure 6. Nearby trajectories (of constant $\mathrm{Im}\,\rho$) must do the same, passing to the sinks on either side; hence there must be a dividing trajectory which must go to infinity.

However, $\rho \sim \lambda$ at infinity, and it follows from this that firstly, the steepest descent trajectories from λ^* asymptote to ∞ horizontally in the left hand part of the plane, and consequently so must also the lines of constant $\mathrm{Im}\,\rho$ which reach infinity from the sinks at $-A_j$. Most of the streamlines from the sources terminate on the adjoining sinks, but the dividing streamline, being sandwiched between adjoining trajectories which originate at $\mathrm{Re}\,\lambda = -\infty$, must also originate there. But this is only possible if $\mathrm{Re}\,\rho$ decreases, and this requires that each dividing streamline from the $J-1$ sources passes through a saddle point, as shown in Figure 6. Since ρ has real-valued coefficients, the phase plane is symmetric about the real axis, so that there are another $J-1$ saddles in the lower half plane.

Together with λ^*, we have accounted for $2J-1$ saddles. This constitutes all of the saddles since direct calculation of ρ' gives

$$\rho'(\lambda) = 1 + v_p \frac{g'(\lambda)}{g(\lambda)} = 0, \tag{3.21}$$

whence the saddles are the $2J-1$ roots of the polynomial

$$\sum_k A_k f_k(\lambda + A_k - v_p) \prod_{l \neq k} (\lambda + A_l)^2 = 0. \tag{3.22}$$

The appropriate choice of v_p follows from the conservation law in (3.16). Clearly the maximum value of ψ_n^j can neither grow nor decay exponentially, and thus we choose v_p such that

$$\rho(\lambda^*) = 0. \tag{3.23}$$

By inspection, we see that this is satisfied, together with (3.21), providing

$$\lambda^* = 0, \quad v_p = \left(\sum_k \frac{f_k}{A_k} \right)^{-1}, \tag{3.24}$$

and thus in the vicinity of the saddle point,

$$\rho(\lambda)t + \xi g(\lambda)\sqrt{t} \approx \frac{1}{2}\rho_0'' \lambda^2 t - \frac{\xi}{v}\lambda\sqrt{t}, \tag{3.25}$$

where $\rho_0'' = \rho''(0)$. Putting $\lambda = is$ gives the local approximation to the steepest descent trajectory, and integrating the resultant approximation to the integral leads to the asymptotic solution

$$\psi_n^j \sim \frac{f_j}{A_j \sqrt{2\pi t \rho_0''}} \exp\left(-\frac{[n_w - v_p t]^2}{2t\rho_0'' v_p^2} \right). \tag{3.26}$$

3.3 Summary of solutions

In summary, we obtained numerical solutions of the basic model in the previous section. Using Laplace transforms we then found that the exact solution of (3.1) and (3.2) for ψ_n^j, the fraction of vacant sites of type j at depth n into the crystal is given by (3.14), incorporating (3.12) and (3.13). For large times, this can be simplified to (3.15) which is inappropriate when $n \sim t$. For large t and $n \sim t$, we then found that the asymptotic limit giving the key result for the penetration n_w of the wavefront into the crystal, at time t, as

$$n_w \sim v_p t, \quad v_p = \left(\sum_k \frac{f_k}{A_k} \right)^{-1}, \tag{3.27}$$

where f_k, A_k are the initial fractions and reaction rates of the species k in the solid. The corresponding asymptotic result for ψ_n^j is given by (3.26).

In the context of Figure 4, the asymptotic solution (3.24) in conjunction with (3.17) predicts that the interface, neglecting its diffusion, moves at a speed $v_p = (\frac{f_1}{A_1} + \frac{f_2}{A_2})^{-1} = 1.54$, that is, $n_w \sim 1.54t$. It is apparent that the individual etchant rates sum like electrical resistors in parallel. The fact that the numerical solutions in Figure 4 are so smooth, and that they are so close to the asymptotic solution, suggests strongly that a continuum model should be appropriate. We now examine this possibility.

4 A continuum model

If we write

$$x = n, \quad \psi^j(x,t) = \psi_n^j, \tag{4.1}$$

then the Gaussian in (3.26) can be represented as the vector solution for $\boldsymbol{\psi} = (\psi^1, \ldots, \psi^J)$,

$$\boldsymbol{\psi} = v_p A^{-1} \mathbf{f} \phi(x,t), \tag{4.2}$$

where $A = \operatorname{diag}(A_j)$, and ϕ satisfies

$$\phi_t + v_p \phi_x = \frac{1}{2} \rho_0'' v_p^2 \phi_{xx}, \quad \phi(x,0) = \delta(x) \tag{4.3}$$

where ρ is defined in (3.25).

It is thus natural to suppose that this result can be found easily and more simply than the earlier discrete calculation, and that it would provide a more suitable vehicle for further development of the model, for example, in considering the shape of the interface on the reaction rates. Consequently, it is surprising to find that a simple continuous approximation apparently fails to reproduce the exact, discrete result.

Before showing why not, it is convenient to rewrite the discrete model and its solution in vector form (which will also indicate the reason why an exact solution is possible). The equations (3.1) with initial conditions (3.2) have the Laplace transformed form

$$\begin{aligned} &(A + \lambda I)\boldsymbol{\Psi}_0 = \mathbf{f}, \\ &(A + \lambda I)\boldsymbol{\Psi}_n = B\boldsymbol{\Psi}_{n-1}, \quad n \geq 1, \end{aligned} \tag{4.4}$$

where $\boldsymbol{\Psi} = (\Psi^1, \ldots, \Psi^J)^T$, and

$$B_{jk} = f_j A_k, \quad A = \operatorname{diag} A_k; \tag{4.5}$$

this has explicit solution

$$\boldsymbol{\Psi}_n = \left\{ (A + \lambda I)^{-1} B \right\}^n (A + \lambda I)^{-1} \mathbf{f}, \tag{4.6}$$

which can also be written in the form

$$\boldsymbol{\Psi}_n = (A + \lambda I)^{-1} \left\{ B (A + \lambda I)^{-1} \right\}^n \mathbf{f}. \tag{4.7}$$

The reason we can find an explicit solution for $\boldsymbol{\Psi}_n$ is because of the separable structure of the components of B. By inspection, one eigenvalue and eigenvector pair of B is

$$\mu = \sum_k f_k A_k, \quad \mathbf{u} = \mathbf{f}, \tag{4.8}$$

and the other eigenvalues are all zero, with the $J - 1$ eigenvectors being spanning vectors for the orthogonal complement $\{\mathbf{a}\}_\perp$ of $\mathbf{a} = (A_1, \ldots, A_J)^T$, that is,

$$\mathbf{u}_i . \mathbf{a}_i = 0, \quad i = 2, \ldots, J. \tag{4.9}$$

As a consequence of this, we have that

$$B\mathbf{v} = (\mathbf{v}.\mathbf{a})\mathbf{f} \tag{4.10}$$

for any vector $\mathbf{v}$ (to see this, write $\mathbf{v}$ as a linear combination of $\mathbf{f}$ and a vector orthogonal to $\mathbf{a}$; or simply do the calculation explicitly). In particular,

$$B(A+\lambda I)^{-1}\mathbf{f} = g(\lambda)\mathbf{f}, \tag{4.11}$$

where

$$g(\lambda) = \left\{(A+\lambda I)^{-1}\mathbf{f}\right\}.\mathbf{a}, \tag{4.12}$$

giving the same definition as in (3.5), and thus (4.7) gives

$$\boldsymbol{\Psi}_n = (A+\lambda I)^{-1} g(\lambda)^n \mathbf{f}, \tag{4.13}$$

in agreement with (3.6).

Now suppose we consider $n = x$ to be continuous. Noting that $w(x-1) = e^{-\partial_x} w(x)$, (4.4) can be written in the form

$$\begin{aligned} \boldsymbol{\Psi} &= (A+\lambda I)^{-1}\mathbf{f} \quad \text{at} \quad x = 0, \\ (A+\lambda I)\boldsymbol{\Psi}(x) &= Be^{-\partial_x}\boldsymbol{\Psi}; \end{aligned} \tag{4.14}$$

Taylor expanding for slowly varying functions of x, thus $e^{-\partial_x} \approx 1 - \partial_x + \frac{1}{2}\partial_{xx}$, this becomes

$$(A+\lambda I)\boldsymbol{\Psi}(x) \approx B\left(\boldsymbol{\Psi} - \boldsymbol{\Psi}_x + \frac{1}{2}\boldsymbol{\Psi}_{xx}\right), \tag{4.15}$$

subject to

$$\begin{aligned} &\boldsymbol{\Psi} = (A+\lambda I)^{-1}\mathbf{f} \quad \text{at} \quad x = 0, \\ &\boldsymbol{\Psi} \to \mathbf{0} \quad \text{as} \quad x \to \infty, \end{aligned} \tag{4.16}$$

the latter being necessary in order that (3.16), which here takes the form

$$\int_0^\infty \|\boldsymbol{\Psi}\|_1 \, dx = 1, \tag{4.17}$$

be satisfied.

Note that in the time domain, (4.15) takes the form

$$\boldsymbol{\psi}_t + B\boldsymbol{\psi}_x = (B-A)\boldsymbol{\psi} + \frac{1}{2}B\boldsymbol{\psi}_{xx}, \tag{4.18}$$

where $\boldsymbol{\psi} = (\psi^1, \ldots, \psi^J)^T$, and bears a suggestive resemblance to (4.3).

The question now arises, how to solve (4.15). We follow the path for the exact equation (4.4), putting

$$\boldsymbol{\Psi} = (A+\lambda I)^{-1}\boldsymbol{\phi}\mathbf{f}, \tag{4.19}$$

from which (4.15) implies

$$\phi = g\left(\phi - \phi_x + \frac{1}{2}\phi_{xx}\right), \tag{4.20}$$

where we would require

$$\begin{aligned} \phi &= 1 \quad \text{at} \quad x = 0, \\ \phi &\to 0 \quad \text{as} \quad x \to \infty. \end{aligned} \tag{4.21}$$

The solution $\phi = \exp[-\{(\frac{2}{g} - 1)^{1/2} - 1\}x]$ to (4.20) simply gives the wrong answer, because there is no basis to neglect the higher derivatives of ϕ in approximating (4.14) by (4.15). In a similar way, the ansatz $\boldsymbol{\psi} \sim v_p A^{-1}\phi\mathbf{f}$ in (4.18) leads to the inconsistent equation

$$A^{-1}\mathbf{f}\phi_t + \mathbf{f}\phi_x = \frac{1}{2}\mathbf{f}\phi_{xx}. \tag{4.22}$$

It seems that only the discrete formulation gives a consistent description of the solution. Nevertheless, the simple form of (4.2) and (4.3) suggests that a derivation of an appropriate advection-diffusion equation should be possible, but it is opaque as to how to do this.

5 Conclusions

In this paper we have developed a model for the etching of a multicomponent lead crystal glass by an acid. In principle, the evolution of the surface is determined by the rate of the surface reaction which dissolves the solid surface. For a single solvent and a monominerallic surface, this rate is determined by the reaction rate kinetics. However, if more than one solvent is necessary to etch a surface with several different components, it is not clear what the effective surface dissolution rate should be. Our approximate solution of what we have called the Tocher conundrum - what is the rate of etching of a surface when multiple reactions are necessary to remove its components - is given by the relation in (3.24),

$$v_p = \left(\sum_j \frac{f_j}{A_j}\right)^{-1}. \tag{5.1}$$

f_j is the proportion of species j in the solid, while A_j is the reaction rate (rate of surface removal) of each species if present on its own. This thus gives an approximation for the overall etching rate, neglecting its diffusion.

In terms of the numerical solutions presented in Figure 4, the basic etching rate is

$$v_p \sim \left(\frac{f_1}{A_1} + \frac{f_2}{A_2}\right)^{-1} = \left(\frac{0.3}{1} + \frac{0.7}{2}\right)^{-1} = 1.54 \tag{5.2}$$

that is, this predicts that $n_w \sim 1.54t$ in Figure 4 where the wavefront n_w is located at the centre of each of the Gaussian-like curves. There is obvious good agreement.

Within the terms of the model we propose, this shows that the solid behaves as if it were layered, with the layers of each species being parallel to the surface, so that the overall rate is determined by the weighted sum of the inverse rates. The constituent etching rates thus sum like electrical resistors in parallel. This surprising conclusion is not at all intuitive, and shows the importance of providing an adequate model for the process.

In addition, we have shown that, although the discrete lattice model has numerical solutions which are smooth at large times, the apparently simple expedient of Taylor expanding the variables and truncating the resulting expansion simply leads to the wrong result. It remains unclear why this should be so, or what the correct averaging method should be to derive an appropriate continuous approximation.

Competing interests

The authors declare that they have no competing interests.

Authors' contributions

The paper is a three way collaboration: the authors have read and approved the final manuscript.

Acknowledgements We acknowledge the support of the Mathematics Applications Consortium for Science and Industry (http://www.macsi.ul.ie) funded by the Science Foundation Ireland mathematics initiative grant 06/MI/005, the Stokes grant 07/SK/I1190 and the PI grant 09/IN.1/I2645.

References

1. Spierings, G.A.C.M.: Wet chemical etching of silicate glasses in hydrofluoric acid based solutions. J. Mater. Sci. **28**, 6261–6273 (1993)
2. Judge, J.S.: A study of the dissolution of SiO_2 in acidic fluoride solutions. J. Electrochem. Soc. **118**, 1772–1775 (1971)
3. Spierings, G.A.C.M., Van Dijk, J.: The dissolution of Na_2O–MgO–CaO–SiO_2 glass in aqueous HF solutions. J. Mater. Sci. **22**, 1869–1874 (1987)
4. Harrison, J.D., Fluri, K., Seiler, K., Fan, Z., Effenhauser, C.S., Manz, A.: Micromachining a miniturized capillary electrophoresis-based chemical analysis system on a chip. Science **261**, 895–897 (1993)
5. Stevens, G.W.W.: Microphotography. Chapman and Hall, London (1968)
6. Macleod Ross, W.: Modern Circuit Technology. Portcullis Press, London (1975)
7. Coombs, J.D.: Printed Circuit Handbook. McGraw-Hill, New York (1979)
8. Fowler, A.C., Ward, J., O'Brien, S.B.G.: A simple model for multi-component etching. J. Colloid Interface Sci. **354**, 421–423 (2011)
9. Tenney, A.S., Ghezzo, M.: Etch rates of doped oxides in solutions of buffered HF. J. Electrochem. Soc. **120**, 1091–1095 (1973)
10. Spierings, G.A.C.M.: Compositional effects in the dissolution of multicomponent silicate glasses in aqueous HF solutions. J. Mater. Sci. **26**, 3329–3336 (1991)
11. Tavassoly, M., Dashtdar, M.: Height distribution on a rough plane and specularly diffracted light amplitude are Fourier transform pair. Opt. Commun. **281**, 2397–2405 (2008)
12. Barabási, A.L., Stanley, H.: Fractal Concepts in Surface Growth. Cambridge University Press, Cambridge (1995)
13. Slikkerveer, P.J., ten Thije Boonkamp, J.H.M.: Mathematical modelling of erosion by powder blasting. Surv. Math. Ind. **10**, 89–105 (2002)

14. Tersoff, J., Tu, Y., Grinstein, G.: Effect of curvature and stress on reaction rates at solid interfaces. Appl. Phys. Lett. **73**(16), 2328–2330 (1998)
15. Kim, K.S., Hurtado, J.A., Tan, H.: Evolution of a surface-roughness spectrum caused by stress in nanometer-scale chemical etching. Phys. Rev. Lett. **83**, 3872–3875 (1999)
16. Yu, H.H., Suo, Z.: Stress-dependent surface reactions and implications for a stress measurement technique. J. Appl. Phys. **87**, 1211–1218 (2000)
17. Kuiken, H.K.: Etching: a two-dimensional mathematical approach. Proc. R. Soc. Lond. Ser. A **392**, 199–225 (1984)
18. Kuiken, H.K.: Etching through a slit. Proc. R. Soc. Lond. Ser. A, Math. Phys. Sci. **396**, 95–117 (1984)
19. Notten, P.H., Kelly, L.H., Kuiken, H.K.: Etching profiles at resist edges. J. Electrochem. Soc. **133**(6), 1226–1232 (1986)